[2]Gravalos, F.G., Edelfelt, I.H., and Emmons, H., "The Supersonic Flow About Blunt Bodies of Revolution for Gases at Chemical Equilibrium," General Electroc Company, Missile and Space Division, TIS R58SD245, June 1959, General Electric Co., Philadelphia, Pa.

[3]Cassanto, J.M., Rogers, D.A., Droms, C.R., and Robison, A.G., "Use of a Miniature Solid State Pressure Transducer for R/V Flight Test Application," *Proceedings of 20th International Instrumentation Symposium*, Albuquerque, N.M., 1974.

[4]Cassanto, J.M., "R/V Flight Test Pressure Instrumentation Techniques," Paper presented at 8th Transducer Workshop, Dayton, Ohio, April 1975.

Effects of Porous Rings on the Aerodynamic Characteristics of a Sphere

George L. Cahen*
Martin Marietta Corporation, Denver Colo.

Nomenclature

A_{ref}	= reference area, $\pi d^2/4$
d	= diameter of sphere
D	= outer diameter of ring
q	= dynamic pressure, $\rho V^2/2$
V	= velocity
C_D	= drag coefficient, drag force / qA_{ref}
C_L	= lift coefficient, lift force / qA_{ref}
C_M	= pitching moment coefficient, pitching moment / $qA_{ref}d$
C_N	= normal force coefficient, normal force / qA_{ref}
α	= angle of attack
σ	= radius of gyration in pitch
$C_{L_\alpha} C_{M_\alpha}, C_{N_\alpha}$	= derivatives with respect to α
$\partial C_M/\partial(\theta d/2V)$ $+\partial C_M/\partial(\dot{\alpha} d/2V)$	= pitch damping coefficient. Overdot implies derivative with respect to time.

Introduction

THE erratic behavior of a sphere in free flight is well known; the fluid mechanical phenomenon—vortex shedding—which is responsible for this behavior is quite well understood. However, to utilize the structural advantage of a sphere for high-pressure planetary entries, it is desirable to improve the stability characteristics and increase its drag coefficient to control the rate of descent. In search of such a solution, Martin Marietta, with NASA's Ames and Langley Research Centers, has tested (both statically and dynamically) a number of concepts. These have included flares, split flares, vented flares, thin rings, both equatorially and post equatorially located, and thick (0.05d), porous rings, equatorially located (originally suggested by NASA Ames Research Center).

The three component static tests measured axial force, normal force and pitching moment in the Martin Marietta, Denver, subsonic wind tunnel. Two types of dynamic tests were conducted. In one the models were mounted on a wire stretched horizontally across the test section of the Army Meteorological Wind Tunnel at Colorado State University so that they were free to pitch through 360°. The other dynamic test was conducted in a vertical wind tunnel (NASA Langley Spin Tunnel) in which the models were free to move in six degrees-of-freedom. Of all configurations tested, the thick porous ring was the most practical. Therefore, this Note will present only the results obtained for that configuration. The effects of ring to sphere diameter ratio, porosity, and center of gravity (c.g.) location on the directional stability and of hole cant angle on the roll rate will be discussed.

Received March 24, 1975; revision received May 27, 1975.
Index categories: Entry Deceleration Systems and Flight Mechanics (e.g., Parachutes); Entry Vehicle Dynamics and Control.

*Senior Group Engineer. Associate Fellow AIAA.

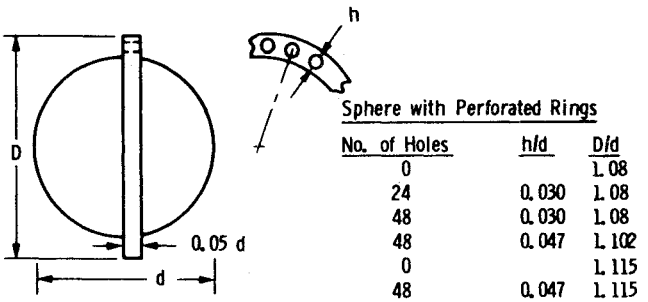

Fig. 1 Configurations tested in the Martin Marietta subsonic wind tunnel.

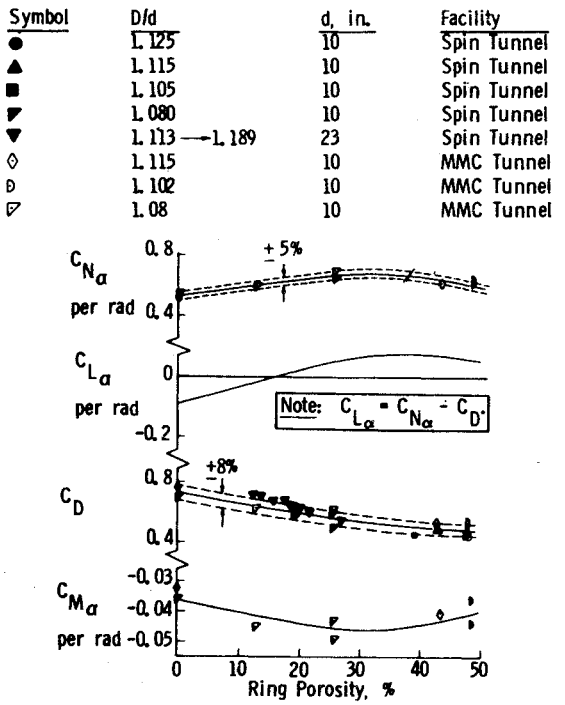

Fig. 2 Summary of aerodynamic derivatives and drag coefficients for zero angle of attack.

Results and Discussion

Static Tests

The configurations for which three component static data were measured are shown in Fig. 1. The sphere model was 10 in. in diameter and constructed of thin (about 1/32 in.) fiberglass reinforced plastic with an aluminum adaptor for sting mounting on a conventional strain gage balance. The porous rings were made of balsa wood. Figure 2 summarized the drag coefficients and the aerodynamic derivatives for $\alpha = 0$ as functions of ring porosity for all configurations tested. Note that, although the data are plotted as functions of porosity, the effects of ring diameter and porosity are both included. For more detailed examination, the pure effect of porosity can be seen for the cases of $D/d = 1.080$ and 1.115. The data show that variations in ring geometry can be used to control the sphere aerodynamic characteristics over a considerable range. The lift curve slope varies with porosity from negative to positive; the drag varies significantly with porosity

Table 1 Results of spin tunnel tests of 10 in. models

Hole configuration	D/d[a]	h/d	c.g. %d	Porosity %ring area	C_D[b] (Ref. D)	Test observations
Effect of c.g. location						
24 at 0.8°	1.125	0.047	−5.0	19.9	0.62	0° trim, 2° perturbations
	1.125	0.047	−3.5	19.9	0.58	0° trim, 4° perturbations
	1.125	0.047	0	19.9	0.62	0° trim, 6° perturbations
Effect of ring diameter and porosity						
24 at 0.8° } 24 at 0	1.125	0.047	−3.5	39.7	0.44	0° trim, 4° perturbations
	1.115	0.047	−3.5	43.4	0.48	0° trim
	1.105	[c]	−3.5	47.7	0.45	0° trim, 3° perturbations
	1.068	[d]	−3.5	37.5	0.35	4° limit cycle
Effect of hole cant angle						
24 at 0.4°	1.125	0.047	−3.5	19.9	0.58	0° trim, 3° perturbations

[a] Variations in ring diameter obtained by cutting back on periphery. [b] Drag coefficient deduced from wind velocity required to sustain model. [c] Ring cut back just to outer edge of holes. [d] Only semicircular holes remain; perimeter of ring wrapped with tape to enclose holes.

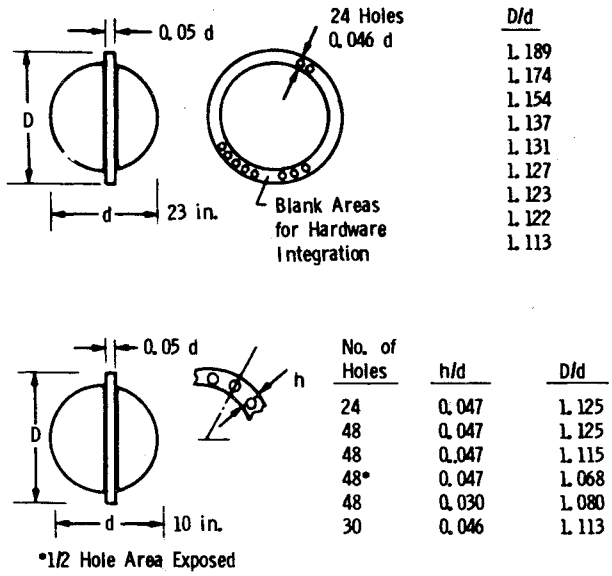

Fig. 3 Configurations tested in the NASA Langley Research Center spin tunnel.

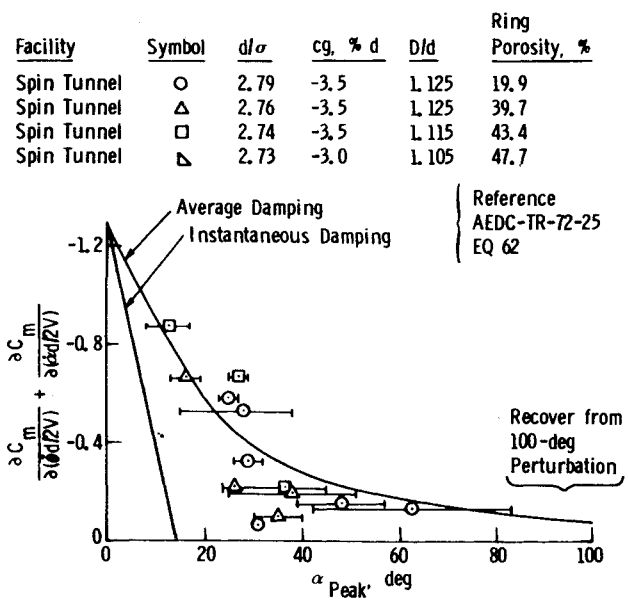

Fig. 4 Pitch damping coefficient as a function of angle of attack.

Table 2 Results of spin tunnel tests of 23 in. models[a]

D/d	c.g. % d	Porosity % Ring Area	C_D (Ref. D)	Test observations
Effect of c.g. location				
1.131	−1.5	18.8	0.64	0° trim, 6° perturbations, weak damping
1.131	−5.0	18.8	0.64	0° trim, 4° perturbations
1.131	−6.5	18.8	0.64	0° trim, 2° perturbations
Effect of ring diameter[b] and porosity				
1.189	−3.5	12.8	0.71	6° half angle limit cycle
1.174	−3.5	13.9	0.70	0° trim, 7° perturbations
1.154	−3.5	15.9	0.68	0° trim, 5° perturbations
1.137	−3.5	18.0	0.68	0° trim, 6° perturbations
1.127	−3.5	19.5	0.63	0° trim, 5° perturbations
1.123	−3.5	20.1	0.62	0° trim, 8° perturbations
1.122	−3.5	20.4	0.62	0° trim, 4° perturbations
1.113	−3.5	22.1	0.60	5° trim, 7° perturbations
1.113[c]	−3.5	27.6	0.54	3° trim

[a] 24 holes, 0.046 d at 0.4° cant angle. [b] Variations in ring diameter obtained by cutting back the ring, leaving the hold pattern undisturbed. [c] 30 holes, 0.046 d at 0.4° cant angle.

(but not with angle of attack to about 30°) and all configurations are statically stable.

Note in Fig. 2 that the drag coefficients vary with porosity from about 0.75 to 0.45. These values indicate that the flowfield configuration is similar to that about a sphere in the subcritical Reynolds number range. That is, the ring forces the flow to separate producing a large wake irrespective of the Reynolds number.

Dynamic Tests

The parameters for the configurations tested in the vertical wind tunnel are shown in Fig. 3. The test procedure was to "float" the models in the wind tunnel by adjusting the wind speed to keep them as nearly in a horizontal plane with the movie camera as possible. Actually, these models flew very steadily so that this task was minimal, requiring only minor adjustments. The models were perturbed by an external force and motion pictures were taken in order to record the dynamic behavior. The models were tracked manually with the camera by virtue of a gimbal mounting. A record of clock time and wind velocity was superimposed into the camera field of view by means of a mirror arrangement.

The movie film was analyzed by reading the angle of the ring relative to the horizontal. The behaviors of the various

configurations are summarized in Tables 1 and 2 for the 10 in. and 23 in. diameter models, respectively. In both tables it is seen that the effect of c.g. location is that more forward locations increase the static stability. This fact is indicated (on the assumption that the disturbances in the wind stream are the same for all models) by the perturbations of the models from the zero degree trim angle reducing as the c.g. is moved forward. In Tables 1 and 2 the effects of ring diameter and porosity are actually inseparable; however, in Table 2, it is seen that for the lowest porosity (largest D/d) a finite limit cycle angle occurred and for the highest porosity (smallest D/d) a finite trim angle occurred, whereas in Table 1, with D/d of 1.105 [which is smaller than the smallest in Table 2 (1.113)] a greater porosity (47.7% compared to 22.1) resulted in changing the trim angle from 5° to 0°. Thus it appears that some minimum value of D/d produces limit cycling which is akin to the behavior of a plain sphere, and some minimum value of porosity produces a finite trim angle. It appears in Table 2 that the effect of increased porosity for the last entry tended to reduce the finite trim angle. The reason for no perturbations for this configuration is not known.

The perturbations indicated in the table do not seem to represent a systematic phenomenon. These perturbations were random in occurrence and are believed to be caused by random turbulence in the wind stream. The drag coefficients from Tables 1 and 2 are compared with the static data in Fig. 2.

Pitch damping coefficients deduced from the Spin Tunnel results for several configurations are shown in Fig. 4. It is interesting that, for these models, the damping coefficient increases strongly as angle of attack approaches zero, whereas, for most high-drag conical configurations, the damping decreases in this range of angle of attack and actually changes sign, resulting in limit cycle behavior. The canted holes in the rings served to effectively control the model roll rate. The roll helix angles measured were actually somewhat greater than the hole cant angles.

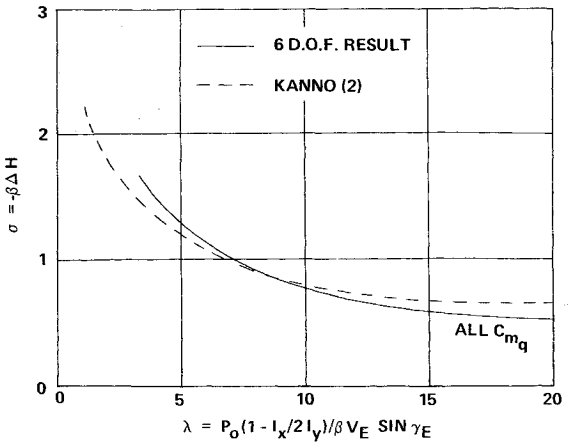

Fig. 1 Nondimensional transient resonance lag at first crossover vs λ.

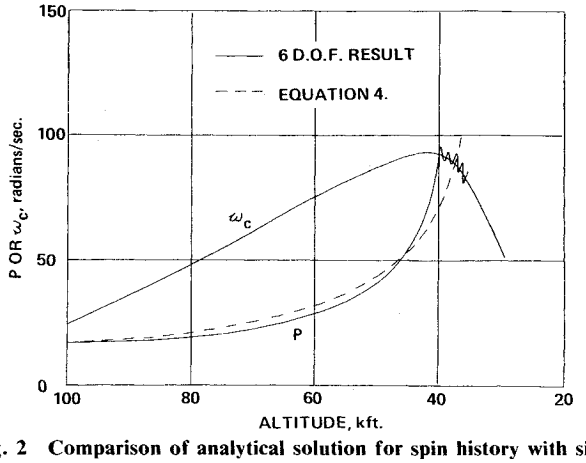

Fig. 2 Comparison of analytical solution for spin history with six-degrees-of-freedom computer results,

Low-Altitude Roll Behavior of Entry Vehicles with Mass Asymmetries

W. J. Bootle*
AVCO Systems Division, Wilmington, Mass.

IT has been shown that a principle axis misalignment and an orthogonal c.g. offset will promote steady resonance in a slender entry vehicle at first intersection of the spin and pitch frequencies whenever the product of the two asymmetries exceeds a critical level K_{cr}.[1] The principle axis tilt is equivalent to a trim angle that is amplified at resonance crossover to produce a roll acceleration $\dot{p}$ that exceeds $\dot{\omega}_c$ and thereby ensures a lock-in.

If the combination is below the critical threshold, the spin rate merely shows a minor fluctuation and then levels off at the initial value p_o, while the angle of attack exhibits the characteristic high-altitude transient resonance divergence. The excursion peak lags the crossover altitude by an interval ΔH that according to a linear analysis by Kanno[2] depends upon the magnitude of the parameter λ where $\lambda = p_o(1 - I_x/2I_y)/\beta V_E \sin\gamma_E$. This interval expressed in the non-dimensional form $\sigma = -\beta\Delta H$ is shown as a function of λ in Fig. 1, where β is the density scale height (22000 ft^{-1}). Six-degrees-of freedom simulations show close agreement with the linear analysis, and also show that to first order the lag is insensitive to C_{m_q}.[3] Typically, ΔH ranges from 5000 to 20000 ft depending on the spin rate and trajectory.

Although a lock-in may not occur, the subsequent spin history is important because this asymmetry combination may still cause a progressive spin up and a second intersection followed by the Pettus[4] type of low-altitude steady resonance to which the vehicle is much more prone because of the larger trim amplification and roll torques. A simple analysis for the spin history following initial crossover will now be presented.

Using the same nomenclature as before,[1] the spin acceleration is written thus:

$$\dot{p} = R\, C_{N_\alpha} q\, S(\alpha_T \Delta y - \beta_T \Delta z)/I_x \tag{1}$$

where R is the amplification ratio and α_T and β_T are the equivalent static trims generated by the principle axis tilt, viz.

$$\alpha_T = -(p/\omega_c)^2 I_{xz}/I_y - I_x \tag{2a}$$

$$\beta_T = -(p/\omega_c)^2 I_{xy}/I_y - I_x \tag{2b}$$

If the damping terms are ignored then $R = 1/(1 - p^2/\omega_c^2)$ (not valid at $p = \omega_c$); over the region of interest $p^2/\omega_c^2 \ll 1$ so we may set $R = 1$ without significant loss of accuracy. Then, substituting for $\omega_c^2 = c_{m\alpha} q\, SD/I_y - I_x$ and noting that $C_{m\alpha} = -C_{N\alpha}\bar{X}/D$ where $\bar{X}$ is the dimensional static margin, Eq. (1) reduces to

$$\dot{p}/p^2 = (-I_{xz}\Delta y + I_{xy}\Delta z)/I_x\bar{X} \tag{3}$$

Received May 5, 1975. This study was performed in part under Air Force Contract AF04(694)-913 (RVTO).

Index categories: Missile Systems; Entry Vehicle Dynamics and Control.

*Senior Consulting Scientist, Vehicle Design Group, Applied Technology Directorate. Member AIAA.